Proceedings of the ASME 2010 10th Biennial Conference on Engineering Systems Design and Analysis
ESDA2010
July 12-14, 2010, Istanbul, Turkey

ESDA2010-24254

DESIGN AND EXPERIMENTAL VALIDATION OF A HARDWARE-IN-THE-LOOP SIMULATOR FOR MECHANISMS WITH LINK FLEXIBILITY

Paolo Boscariol*
Department of Electrical, Managerial and Mechanical Engineering
University of Udine
Udine, Italy 33100
Email: paolo.boscariol@uniud.it

Alessandro Gasparetto
Department of Electrical, Managerial and Mechanical Engineering
University of Udine
Udine, Italy 33100
Email: gasparetto@uniud.it

Vanni Zanotto
Department of Electrical, Managerial and Mechanical Engineering
University of Udine
Udine, Italy 33100
Email: vanni.zanotto@uniud.it

ABSTRACT

The aim of this paper is to demonstrate the capabilities and potential of a Hardware-In-the-Loop (HIL) simulator for the tuning of closed-loop control strategies used in flexible-links mechanisms. HIL is an increasingly popular methodology used in reducing the design and validation time of complex systems. This approach makes use of a software-programmed hardware prototype of the device under test, which is able to interact with other hardware devices and real-world signals. In this paper a validation of the proposed simulator, named FLiMHILS (Flexible Link Mechanisms HIL Simulator), will be obtained by comparing the dynamic behavior of a real single-link mechanism with the corresponding response of the simulator subject to the same stimuli and controller parameters. The experimental results show how the tuning parameters obtained with the HIL simulator can be successfully used to control the real mechanism. The real-time capable model which constitutes the core of the HIL simulator is a highly accurate FEM-based nonlinear model capable of describing with consistency the dynamics of different planar mechanisms with flexible links.

NOMENCLATURE

$\{X,Y,Z\}$ Global reference frame
$\mathbf{r}_i$ Vector of nodal position of the i-th element of the ERLS
$\mathbf{u}_i$ Vector of nodal displacement of the i-th element of the ERLS
$\mathbf{p}_i$ Position of a generic point inside the i-th element of the ERLS
$\mathbf{q}$ Vector of generalized coordinates of the ERLS
ε_i Strain vector
$\mathbf{D}_i$ Stress-strain matrix
ρ_i Mass density of the i-th link
$\mathbf{F}$ Vector of external forces acting on the mechanism
$\mathbf{T}_i$ Global-to-local transformation matrix
$\mathbf{R}_i$ Local-to-global transformation matrix
$\mathbf{N}_i$ Shape function matrix
$\mathbf{B}_i(x_i,y_i,z_i)$ Strain-displacement matrix
$\delta\mathbf{u}$ Nodal elastic virtual displacements
$\delta\mathbf{r}$ Nodal virtual displacements of the ERLS
$\mathbf{M}$ Mass matrix
$\mathbf{S}$ Sensitivity coefficient matrix
$\mathbf{M}_G$ Matrix of Coriolis contributions
$\mathbf{K}$ Stiffness matrix
α,β Rayleigh damping coefficients
$\mathbf{E}$ Young's modulus
$\mathbf{EJ}$ Flexural stiffness
$\mathbf{a},\mathbf{b}$ Beam thickness and width
s Strain sensor position
$\mathbf{A},\mathbf{B},\mathbf{C},\mathbf{D}$ Matrices that define the linearized state-space model of the mechanism

*Address all correspondence to this author.

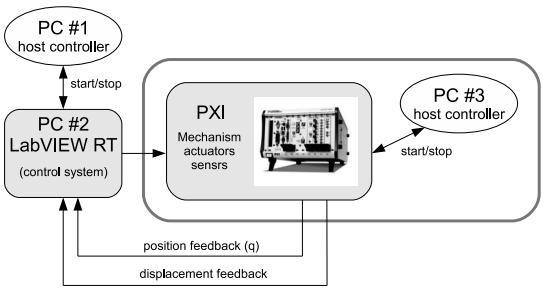

FIGURE 1. EXPERIMENTAL TESTS: HIL APPROACH

L State observer gain matrix

INTRODUCTION

The study of accurate models for flexible link manipulators (FLM) is a field that has attracted a great deal of interest among researchers. This is due to the fact that the ability to accurately model and control the vibrational phenomena in mechanisms can be directly translated into the development of robots with both lighter arms and a higher ratio between their maximum load and overall weight. Smaller arms also means a reduction in their inertia value, with a positive influence on the operative speed of manipulators. In the wake of these possibilities, in the past four decades a lot of papers and books have been written to propose and investigate both innovative dynamic models and control strategies. A comprehensive review of the work done in this area can be found in [1]. On the other hand, the experimental tests of control strategies for vibration reduction in flexible-link mechanism pose some technical problems. FLM are quite prone to mechanical failures, which are encountered when the links are subject to strong strains as a consequence of an improper control strategy. This is especially true when dealing with closed-loop mechanisms. This also represents a potential safety risk for the operator. One solution to these problems can be found in Hardware-In-the-Loop (HIL) tests. This technology allows the complete and accurate interaction of a real device with a simulated one.

In this case a software that implements a virtual model of the dynamics of a flexible-link mechanism can be run on a PC-based device and, through an interface board, interaction with a real control system can be established, as shown in Fig. 1. By using this methodology, a large number of experimental tests required for the tuning of the control system parameters can run without involving the fragile mechanism prototype, as shown in Fig. 2. Other advantages of the HIL approach include:

- reproducibility of experiments
- the ability to perform tests which would otherwise be impossible, impractical and unsafe
- shorter time required for experimental testing

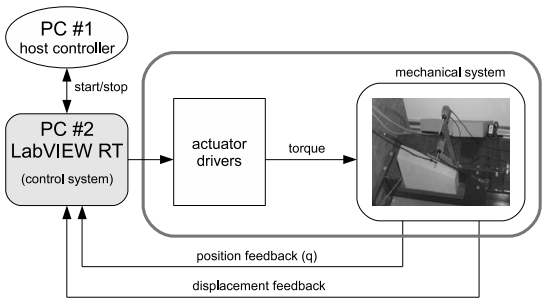

FIGURE 2. EXPERIMENTAL TESTS: TRADITIONAL APPROACH

- testing the effects of component faults
- long-term durability testing

Hardware-In-the-Loop technology is experiencing a wide diffusion in many industrial fields, in the wake of its early but successful introduction in the aerospace [2] and automotive [3] research areas. More recently many papers have been written on the subject of HIL simulator for mechatronic systems, such as [4, 5] on the use of HIL in machine tool design, [6] on the design of mobile robots and [7–9] on the analysis and synthesis of robotic systems. However, to the authors' best knowledge, there are no papers available in literature on the development or the use of Hardware-In-the-Loop simulators for mechanisms with link flexibility. One requirement of the dynamic model employed for HIL is its real-time capability, since it is necessary to make it interact with real-world signals, as the input and outputs of the control system employed in the feedback loop. This is a problem without an easy solution, since the dynamic model used is both non-linear and high order, i.e., it involves large and badly conditioned matrices whose computation requires a large amount of resources [10]. Moreover, the structure of the equation of motion and the parameters of the model make the equation of motion ill-conditioned.

In the first part of the paper a brief explanation of the dynamic model of flexible link mechanisms will be given, then some details of its real-time implementation will be introduced. The characteristics of the test bench are exposed in detail in the following section, and after that the experimental results are presented. The validation of the Hardware-In-the-Loop simulator is conducted by comparing the response of the HIL simulator, using a PID position control and a LQR optimal position and vibration control, with the response of the real flexible-link mechanism using the very same Real-Time controllers. Here two well-known control strategies are applied to the simplest flexible-link mechanism, but the authors' aim is to address their future work to extending the capabilities of the proposed simulator to the closed-chain 4-link FLM already analyzed in [11] and to employ such a simulator to test the capabilities of the Model-Predictive Control proposed in [12].

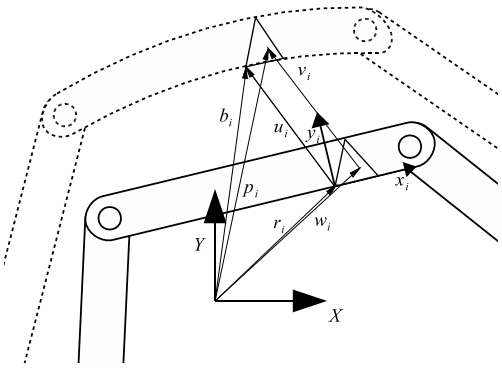

FIGURE 3. KINEMATIC DEFINITIONS

DYNAMIC MODEL OF A PLANAR FLEXIBLE-LINKS MECHANISM

In this section the dynamic model of a flexible-link mechanism proposed by Giovagnoni [13] will be briefly outlined. This introduction is meant to give an insight of the model, which can be useful to better understand the complexity of the software implementation of the Hardware-In-the-Loop simulator. The choice of this formulation among the several proposed in the last 40 years has been motivated mainly by the high grade of accuracy provided by this model, which has been proved several times: for example in [14–16].

Each flexible link belonging to the mechanism is divided into finite elements. Referring to Fig. 3, the following vectors, calculated in the global reference frame $\{X,Y,Z\}$, can be defined:

- $\mathbf{r}_i$ and $\mathbf{u}_i$ are the vectors of the nodal position and nodal displacement in the ith element of the ERLS, and of their elastic displacement
- $\mathbf{p}_i$ is the position of a generic point inside the ith element
- $\mathbf{q}$ is the vector of the generalized coordinates of the ERLS

Applying the principle of virtual work, the following relation can be stated:

$$\begin{aligned}&\sum_i \int_{V_i} \delta\mathbf{p}_i{}^T \ddot{\mathbf{p}}_i \rho_i dv + \sum_i \int_{V_i} \delta\varepsilon_i{}^T \mathbf{D}_i \varepsilon_i dv \\ &= \sum_i \int_{V_i} \delta\mathbf{p}_i{}^T \mathbf{g}\rho dv + (\delta\mathbf{u}^T + \delta\mathbf{r}^T)\mathbf{F}\end{aligned} \tag{1}$$

ε_i, $\mathbf{D}_i$, ρ_i and $\delta\varepsilon_i$ are, respectively, the strain vector, the stress-strain matrix, the mass density and the virtual strains of the ith link. $\mathbf{F}$ is the vector of the external forces, including gravity, whose acceleration vector is $\mathbf{g}$. Eqn. 1 shows the virtual works of, respectively, inertia, elastic and external forces. From this equation, $\delta\mathbf{p}_i$ and $\ddot{\mathbf{p}}_i$ for a generic point in the ith element are:

$$\begin{aligned}\delta\mathbf{p}_i &= \mathbf{R}_i\mathbf{N}_i\mathbf{T}_i\delta\mathbf{r}_i \\ \ddot{\mathbf{p}}_i &= \mathbf{R}_i\mathbf{N}_i\mathbf{T}_i + 2(\dot{\mathbf{R}}_i\mathbf{N}_i\mathbf{T}_i + \mathbf{R}_i\mathbf{N}_i\dot{\mathbf{T}}_i)\dot{\mathbf{u}}_i\end{aligned} \tag{2}$$

where $\mathbf{T}_i$ is a matrix that describes the transformation from the global-to-local reference frame of the ith element, $\mathbf{R}_i$ is the local-to-global rotation matrix and $\mathbf{N}_i$ is the shape function matrix. Taking $\mathbf{B}_i(x_i,y_i,z_i)$ as the strain-displacement matrix, the following relation holds:

$$\delta\varepsilon_i = \mathbf{B}_i\delta\mathbf{T}_i\mathbf{u}_i + \mathbf{B}_i\mathbf{T}_i\delta\mathbf{u}_i \tag{3}$$

Since the nodal elastic virtual displacements ($\delta\mathbf{u}$) and nodal virtual displacements of the ERLS ($\delta\mathbf{r}$) are independent from each other, the resulting equation describing the motion of the system is:

$$\begin{bmatrix}\mathbf{M} & \mathbf{MS} \\ \mathbf{S}^T\mathbf{M} & \mathbf{S}^T\mathbf{MS}\end{bmatrix}\begin{bmatrix}\ddot{\mathbf{u}} \\ \ddot{\mathbf{q}}\end{bmatrix} = \begin{bmatrix}\mathbf{f} \\ \mathbf{S}^T\mathbf{f}\end{bmatrix} \tag{4}$$

$\mathbf{M}$ is the mass matrix of the whole system and $\mathbf{S}$ is the sensitivity matrix for all the nodes. Vector $\mathbf{F} = \mathbf{F}(\mathbf{u},\dot{\mathbf{u}},\mathbf{q},\dot{\mathbf{q}})$ takes into account all the forces affecting the system, including the force of gravity. Adding a Rayleigh damping, the right-hand side of Eqn. 4 becomes:

$$\begin{aligned}\begin{bmatrix}\mathbf{f} \\ \mathbf{S}^T\end{bmatrix} &= \begin{bmatrix}-2\mathbf{M}_G - \alpha\mathbf{M} - \beta\mathbf{K} & -\mathbf{M}\dot{\mathbf{S}} & -\mathbf{K} \\ \mathbf{S}^T(-2\mathbf{M}_G - \alpha\mathbf{M}) & -\mathbf{S}^T\mathbf{M}\dot{\mathbf{S}} & 0\end{bmatrix}\begin{bmatrix}\dot{\mathbf{u}} \\ \dot{\mathbf{q}} \\ \mathbf{u}\end{bmatrix} \\ &+ \begin{bmatrix}\mathbf{M} & \mathbf{I} \\ \mathbf{S}^T\mathbf{M} & \mathbf{S}^T\end{bmatrix}\begin{bmatrix}\mathbf{g} \\ \mathbf{F}\end{bmatrix}\end{aligned} \tag{5}$$

Matrix $\mathbf{M}_G$ accounts for the Coriolis contribution, while $\mathbf{K}$ is the stiffness matrix of the whole system. α and β are the two Rayleigh damping coefficients. The system in (4) and (5) can be made solvable by forcing to zero as many elastic displacements as there are generalized coordinates, and in this way the ERLS position is defined univocally [13]. Finally, after removing the displacement forced to zero from (4) and (5) one obtains:

$$\begin{bmatrix}\mathbf{M}_{in} & (\mathbf{MS})_{in} \\ (\mathbf{S}^T\mathbf{M})_{in} & \mathbf{S}^T\mathbf{MS}\end{bmatrix}\begin{bmatrix}\ddot{\mathbf{u}}_{in} \\ \ddot{\mathbf{q}}\end{bmatrix} = \begin{bmatrix}\mathbf{f}_{in} \\ \mathbf{S}^T\mathbf{f}_{in}\end{bmatrix} \tag{6}$$

HIL IMPLEMENTATION

The purpose of the Hardware-In-the-Loop simulator is to achieve an interaction between a real implementation of a closed-loop control system and a simulated plant. The model used for HIL requires the accomplishment of two targets: (a) *high accuracy* (b) *Real-Time capability*. The high accuracy of the model has been proved, as already stated, in several papers by comparing the results of experimental tests with the evidence of off-line simulation, as in [17]. The need for a deterministic system arises from the use of both real and simulated hardware. The model running on the Real-Time target has to respect a condition of time constraint condition, or in other words, should have a constant refresh frequency. From Eqn. (6), which can be rewritten as:

$$\mathbf{M}(\mathbf{x},t)\dot{\mathbf{x}} = f(\mathbf{x},t,\mathbf{u}) \tag{7}$$

it can be seen that it involves a large, non linear and time dependent matrix $\mathbf{M}(\mathbf{x},t)$. The calculation of the update vector $\dot{\mathbf{x}}$ in this case requires the numerical inversion of such matrix, so the resulting model cannot be run fast enough for Real-Time execution on a standard PC. It must be considered that the proposed HIL simulator allows the user to chose the number of finite elements to employ. For this reason the size of matrix $\mathbf{M}(\mathbf{x},t)$ goes from 8×8 to 32×32 since it can be chosen to describe the link with a number of flexible finite elements ranging from 1 to 5.

The proposed solution to considerably speed up the calculation of $\dot{\mathbf{x}}$ at each step is to make this vector explicit using the symbolic formula:

$$d\mathbf{x} = \mathbf{M}^{-1}(\mathbf{x},t)\, f(\mathbf{x},t,\mathbf{u}) \tag{8}$$

An optimized C-code Matlab routine implementation of Eqn. (8) has been used for developing real-time (or even faster than real-rime) simulated capability. The speed-up advantage is due to the lack of online power-hungry operations such as matrix inversion, since the calculus of $\mathbf{M}^{-1}(\mathbf{x},t)$ can be operated off-line. The main drawback of this approach is that a large amount of memory allocation is required for the symbolic computation of the inverse of the $\mathbf{M}(\mathbf{x},t)$ matrix. It should however be pointed out that this calculation must be performed only once during the design of the simulator.

A PXI system has been chosen as the hardware platform used for the real-time simulation of the whole system, including sensors and actuators drivers. It integrates a standard PC-based CPU with high a performance I/O board, so it is well suited for both control and measurement application. The HIL simulator has been implemented on a 1042Q PXI chassis using the PXI-8186 controller and the analog I/O board PXI-6259, all produced by National Instruments®. The executable file, originally written in C language, can be included in a LabVIEW VI that can be deployed on the PXI, where it can run on a real-time OS. The model's refresh frequency can be chosen by the user: for all the experimental tests presented in this paper it has been set to 1 kHz. As it will be shown in the following sections, this sampling frequency is sufficient to describe with accuracy the main dynamics of the flexible link.

TABLE 1. STRUCTURAL AND DYNAMIC CHARACTERISTICS OF THE FLEXIBLE ROD

	Symbol	Value
Young's modulus	E	$210\cdot 10^{9}$ [Pa]
Flexural stiffness	EJ	166.67 [Nm^4]
Beam width	a	$1\cdot 10^{-2}$ [m]
Beam thickness	b	$1\cdot 10^{-2}$ [m]
Mass/unit length	m	0.7880 [kg/m]
Flexible Link length	l	1.4 [m]
Strain sensor position	s	0.7 [m]
First Rayleigh damping constant	α	$8.7\cdot 10^{-2}$ [s^{-1}]
Second Rayleigh damping constant	β	$2.1\cdot 10^{-5}$ [s^{-1}]

REFERENCE MECHANISM

A single-link flexible mechanism has been chosen as the reference model is a single-link flexible mechanism. It is composed by a square-section metal rod actuated by a brushless motor, so it can swing along the vertical plane. The beam can be modeled as a single dof mechanism, since its position depends only on the angular position q. A picture of the mechanism prototype used for the experimental tests can be seen in Fig. 4.

The choice of a suitable number of flexible finite elements to describe accurately the elastic behavior of the mechanism has been based on experimental evidence. An evaluation of the prominent modes of the flexible rod has been deduced by analyzing the spectrum of the vibrations when the rod is excited by tapping its end with a steel hammer. This experimental data is then compared with the response of the HIL simulator to the same kind of stimulus. Such conditions can be reproduced by blocking the rotation of the rigid degree of freedom $\mathbf{q}$ and introducing a sequence of impulsive forces on the last node of the FLM. The results of this comparison is shown in Fig. 5. The black trace represents the FFT of the strain signal, which has been acquired

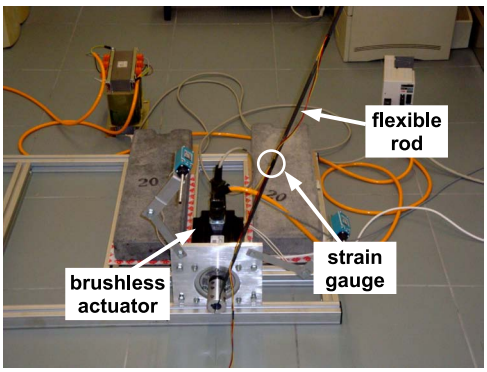

FIGURE 4. THE MECHANISM USED FOR EXPERIMENTAL TESTS

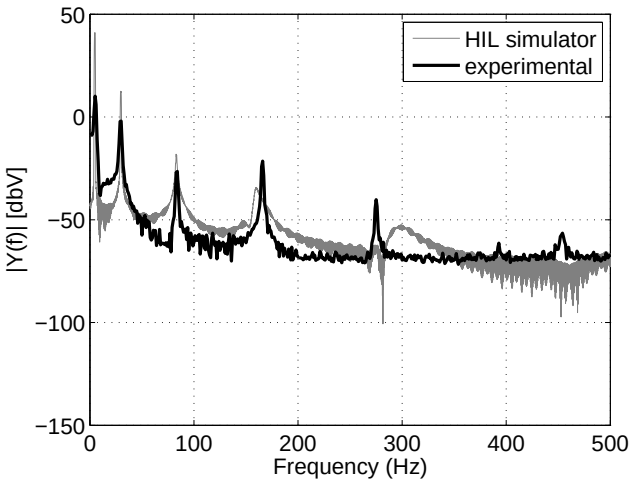

FIGURE 5. FREQUENCY SPECTRUM OF STRAIN SIGNAL: COMPARISON BETWEEN EXPERIMENTAL RESULTS AND HIL SIMULATION

with a Hottinger Baldwin Messtechnik KWS 3073 strain gauge amplifier. The gray trace represents the FFT of the angular elastic displacement of the node located at the midspan of the flexible link. Several tests have been conducted to choose the optimal number of finite elements, and in this case 4 flexible elements have been chosen to describe the link. As can be seen in Fig. 5 the HIL simulator has the ability to describe with negligible errors the first three modes of the real mechanism (4.5 Hz, 28 Hz, 81 Hz) and, with lesser but still sufficient precision, the modes located at 167 Hz and 274 Hz. It should be pointed out that the modes of high order are less important for the description of the elastodynamics of FLM, since they have a very fast decay time. As such, the resulting vector of nodal displacements is composed by 12 elements:

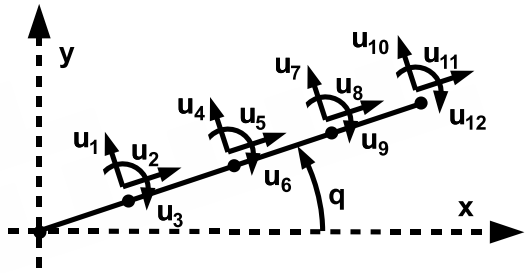

FIGURE 6. FEM DISCRETIZATION: NODAL DISPLACEMENTS

$$\mathbf{u} = \left[u_1 \; u_2 \; u_3 \; \ldots \; u_{11} \; u_{12} \right]' \tag{9}$$

The measured strain can be directly linked to the angular displacement u_6, located at the third node of the finite element chain, as it can be seen in Fig. 6. From this choice of finite elements, the state vector $\mathbf{x}$ in Eqn. (5) has 26 components, and the size of the matrix that needs to be inverted in Eqn. (6) is 26×26.

EXPERIMENTAL RESULTS

In order to verify the accuracy of the dynamic model in HIL configuration, a comparison between the response of the mechanism obtained in the HIL environment and the measured response of the mechanism prototype will be set with the same control parameters. This comparison has to be done using a closed-loop control system, since the gravity force acting on the mechanism and the limited movement range of the mechanism does not allow to operate the plant in open-loop mode. Moreover, the purpose of the proposed HIL simulator is to use it as a flexible and robust test bench for position and vibration control systems of flexible-links mechanisms. The tests have been conducted in this way: first a tuning of the control systems (a PID position control and an optimal LQR position and vibration control) has been done using the real-time control system and the HIL simulator. Following this the same control system, with exactly the same gains and tuning parameters, is applied to the real mechanism.

PID POSITION CONTROL

The experimental results presented in Fig. 8-13 show the comparison between the response of the HIL simulator and the real FLM mechanism, using the PID position control together with a nonlinear feedback gravity compensation block, configured as in Fig. 7.

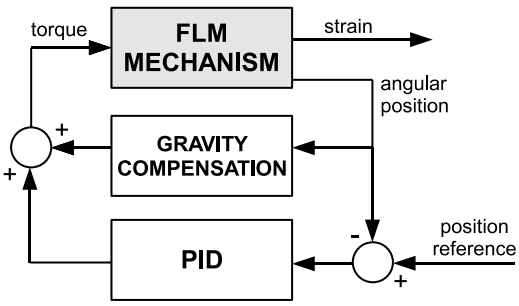

FIGURE 7. PID POSITION CONTROL WITH GRAVITY FEEDBACK COMPENSATION

In Fig. 8 the two torques applied to the HIL simulator and to the mechanism prototype are reported, and in Fig. 9-10 a more detailed view of the two transients can be found. In all the following graphs, the response of the HIL simulator is plotted with a grey line, while the plot relative to the real system is represented with a black solid line. The initial position of the mechanism is $q = 90$ deg, then the reference signal goes to 80 degrees at constant speed, and then to 85 degrees. As can be seen in these graphs, there is high level of likeness between the two simulations, meaning that the HIL simulator has the ability to reproduce the evolution of the real system. In Fig. 10 and in a less evident amount also in Fig. 11, the effects of the encoder bouncing can be seen. This effect has not yet been introduced in the HIL simulator, but from the experimental evidence it can be seen that this phenomenon has a very limited influence on the response of the plant. The angular position signal is generated from a quadrature encoder with a resolution of 4000 CPR mounted on the motor shaft. The torque provided to the HIL simulator and the motor drivers are plotted and compared in Fig. 11. The two profiles are almost identical, meaning that the effects of gravitational force and torque are clearly modeled in the HIL simulator.

In Fig. 12-14 the comparison of the signal produced by the strain gauge amplifier is compared to the angular displacement produced by the HIL simulator. A gain factor of around 93 has been introduced in the HIL simulator in order to convert a signal which is originally measured in radians to the voltage provided by the strain gauge amplifier. This conversion factor has been deduced from an extended set of measurements conducted on the real mechanism by reading the strain voltage in different steady positions of the mechanism. This sequence of values has been compared to the strain measured on the HIL simulator in the same configurations, and a correct gain factor has been deducted. This procedure ensures a reliable calibration of the strain signal. As it can be seen in Fig. 12-14 the likeness of the two responses is remarkable. In order to show more clearly the small differences between the two signals, a detailed view of the strain during the two position transients are presented in Fig. 13-14.

All the experimental evidence presented in Fig 8-14 confirm

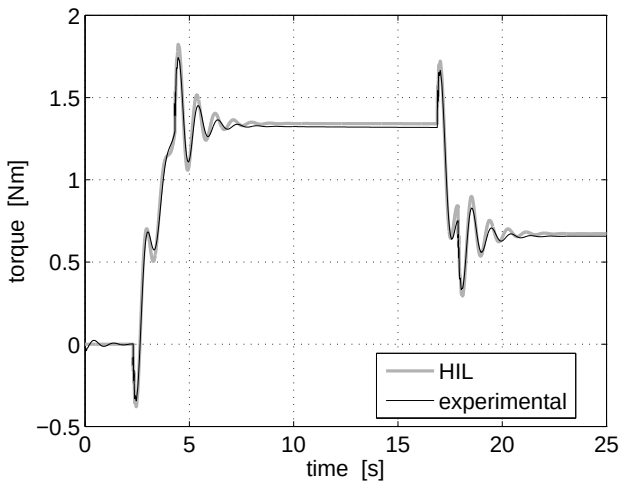

FIGURE 8. PID CONTROL: HIL VS. EXPERIMENTAL RESULTS - APPLIED TORQUE

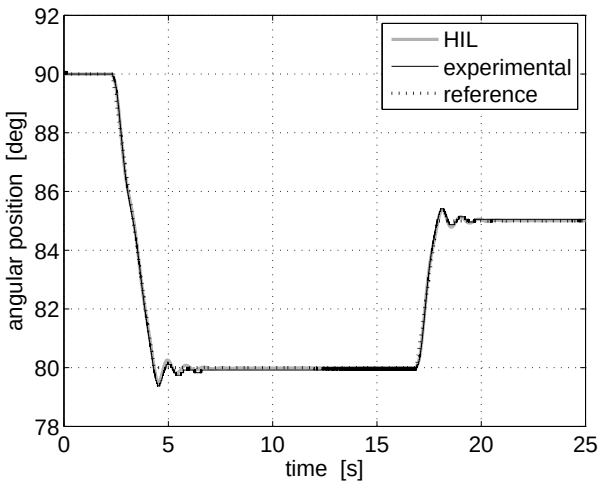

FIGURE 9. PID CONTROL: HIL VS. EXPERIMENTAL RESULTS - ANGULAR POSITION **q**

that the HIL simulator can faithfully mimic the response of the real FLM, and that the tuning of a PID control system conducted on the Hardware-In-the-Loop simulator can be applied successfully to the mechanism prototype.

LQR POSITON AND VIBRATION CONTROL

In this section further proof of the accuracy of the Hardware-In-the-Loop simulator is given, by comparing the responses of the HIL test bench and the real mechanism using a LQR position and vibration control, together with a feedback gravity compensation block. A graphic representation of the control's loop

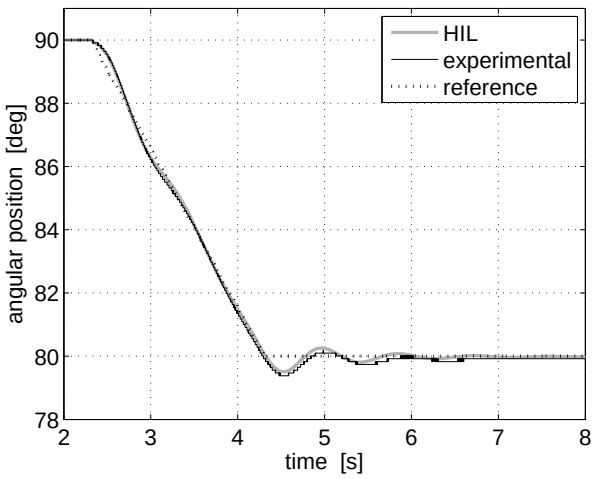

FIGURE 10. PID CONTROL: HIL VS. EXPERIMENTAL RESULTS - ANGULAR POSITION **q**, DETAILED VIEW OF FIRST TRANSIENT

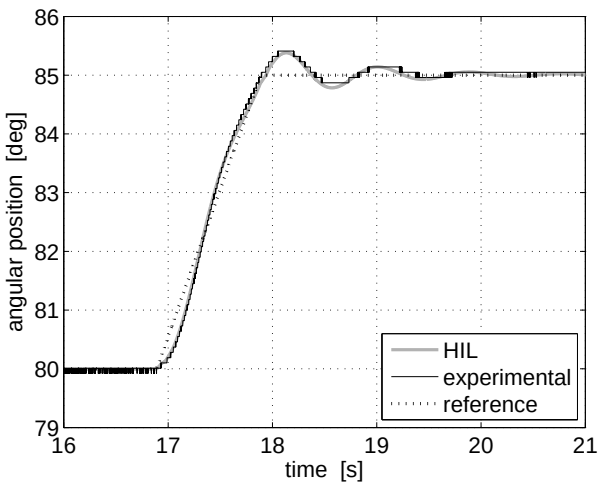

FIGURE 11. PID CONTROL: HIL VS. EXPERIMENTAL RESULTS - ANGULAR POSITION **q**, DETAILED VIEW OF SECOND TRANSIENT

structure of the control loop is reported in Fig. 15. Owing to the space constraints of this paper, just a basic overview of this controller will be given: for more references see [18]. The LQR control calculates the optimal control sequence $\tau(t)$ which maximizes the performance index **J** calculated as:

$$\mathbf{J} = \int_0^\infty \left[\mathbf{x}(t)\mathbf{Q}\mathbf{x}(t) - \tau^T(t)\mathbf{R}\tau(t)\right] dt \qquad (10)$$

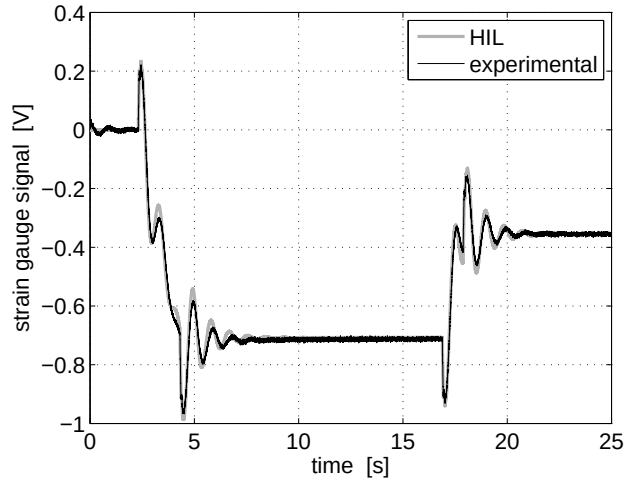

FIGURE 12. PID CONTROL: HIL VS. EXPERIMENTAL RESULTS - STRAIN GAUGE SIGNAL

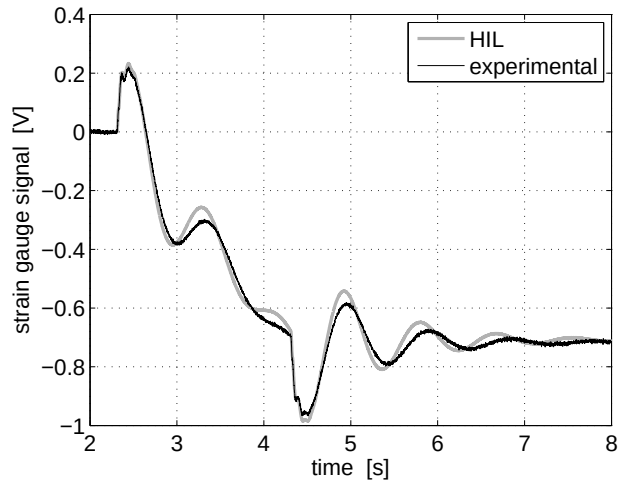

FIGURE 13. PID CONTROL: HIL VS. EXPERIMENTAL RESULTS - STRAIN GAUGE SIGNAL, DETAILED VIEW OF FIRST TRANSIENT

The first term inside the integral minimizes the absolute value of the nodal displacements, the free coordinate q and their velocity, whereas, the second takes into account the absolute value of the system input (in this case the torque τ applied to the flexible link). **Q** and **R** are diagonal matrices of weight: the first one refers to the controlled variables, the latter refers to the control variable. In this case, there are only 2 controlled variables, the angular position q and the elastic displacement at the midspan of the rod. Matrix **R** is simply a scalar, since there is only one control variable. The resulting optimal control sequence can be expressed in matrix form as:

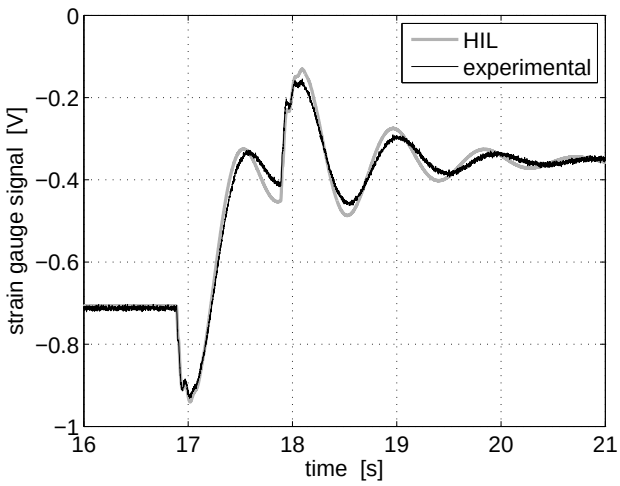

FIGURE 14. PID CONTROL: HIL VS. EXPERIMENTAL RESULTS - STRAIN GAUGE SIGNAL, DETAILED VIEW OF SECOND TRANSIENT

$$\tau(t) = -\mathbf{K}\mathbf{x}(t) \tag{11}$$

where the optimal value of the gain matrix $\mathbf{K}$ is given by:

$$\mathbf{K} = \mathbf{R}^{-1}\mathbf{G}^T\mathbf{P} \tag{12}$$

$\mathbf{P}$ can be obtained by solving Riccati's equation, being $\mathbf{A}$, $\mathbf{B}$, $\mathbf{C}$, $\mathbf{D}$ the matrices that define a state-space model of the LTI plant to control:

$$-\mathbf{A}^T\mathbf{P} - \mathbf{P}\mathbf{A} + \mathbf{P}\mathbf{G}\mathbf{L}^{-1}\mathbf{B}^T\mathbf{P} - \mathbf{C}^T\mathbf{Q}\mathbf{C} = 0 \tag{13}$$

Such a linear state-space model has been obtained by applying a linearization procedure applied to Eqn (5). The control strategy explained above can be applied only when a measure of the whole state $\mathbf{x}$ is available. In this application, there are only two measured values, so a state observer must be used.

Here a standard Kalman asymptotic estimator has been chosen. An estimation of $\mathbf{x}(k)$ and $\mathbf{x}_m(k)$ (where $\mathbf{x}(k)$ is the state of the plant model and $\mathbf{x}_m(k)$ is the state of the measurement noise model) can be computed from the measured output $\mathbf{y}_m(k)$ through:

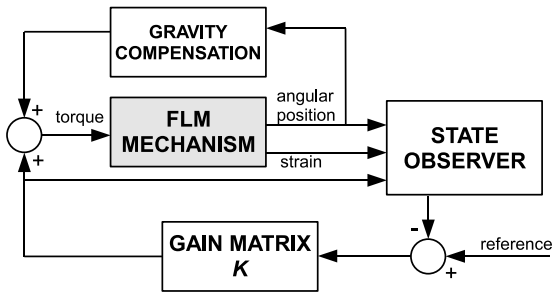

FIGURE 15. LQR POSITION AND VIBRATION CONTROL WITH GRAVITY FEEDBACK COMPENSATION

$$\begin{bmatrix} \hat{\mathbf{x}}(k|k) \\ \hat{\mathbf{x}}_m(k|k) \end{bmatrix} = \begin{bmatrix} \hat{\mathbf{x}}(k|k-1) \\ \hat{\mathbf{x}}_m(k|k-1) \end{bmatrix} + \mathbf{L}(\mathbf{y}_m(k) - \hat{\mathbf{y}}_m(k))$$

$$\begin{bmatrix} \hat{\mathbf{x}}(k+1|k) \\ \hat{\mathbf{x}}_m(k+1|k) \end{bmatrix} = \begin{bmatrix} \mathbf{A}\hat{\mathbf{x}}(k|k) + \mathbf{B}_u\mathbf{u}(k) \\ \tilde{\mathbf{A}}\hat{\mathbf{x}}_m(k|k) \end{bmatrix} \tag{14}$$

$$\hat{\mathbf{y}}_m(k) = \mathbf{C}_m\hat{\mathbf{x}}(k|k-1)$$

The gain matrix $\mathbf{L}$ is designed using Kalman filtering techniques, see [18]. The response of the HIL simulator and of the mechanism when the LQR position and vibration control is used are reported in Fig. 16-20. The initial position of the mechanism is 72 deg., the final position is 90 deg. and such a rotation is performed in 3 s. As is evident, the LQR control strategy can be very effective for vibration damping: the angular position q is tracked with good precision (although with short delay), as in Fig. 16-17, and the elastic deformations of the link are quite limited and very well damped: vibration is practically reduced to zero, just after the mechanism has reached the final angular position. Again, the experimental comparison established in Fig. 16-20 gives additional proof of the accuracy of the Hardware-In-the-Loop simulator. It should be noted that the LQR controller used in these tests requires for the HIL simulator to have a higher level of accuracy comparing to the requirements of PID control, since it also relies on elastic displacement for the evaluation of both the estimated state and the optimal torque value.

CONCLUSION

An efficient way to compute real-time capable and highly accurate dynamic model of the flexible-link mechanism has been presented in this paper. This model has been employed to create an HIL test system based on PXI hardware platform. The accuracy of such a simulator has been shown through several examples of experimental evidence. First a comparison of the vibration modes of the mechanism and of the HIL simulator has been

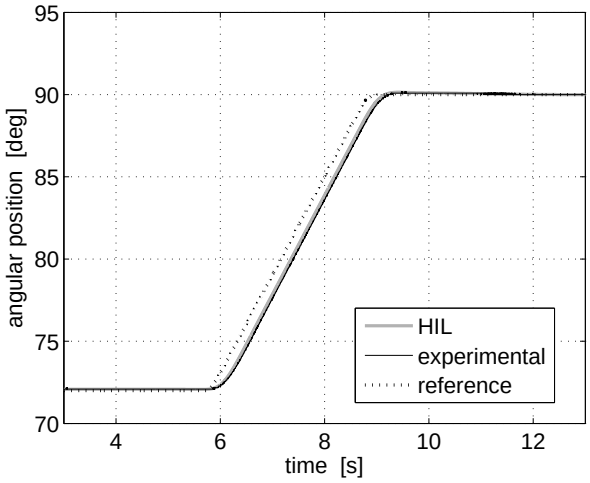

FIGURE 16. LQR CONTROL: HIL VS. EXPERIMENTAL RESULTS - ANGULAR POSITION **q**

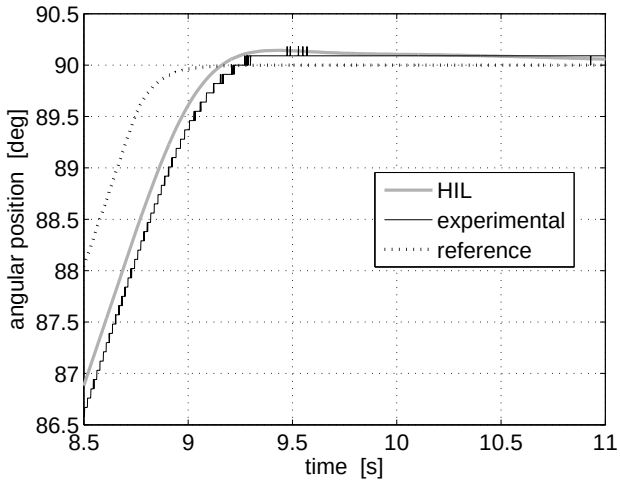

FIGURE 17. LQR CONTROL: HIL VS. EXPERIMENTAL RESULTS - ANGULAR POSITION **q**, DETAILED VIEW OF SECOND TRANSIENT

set. Then the response of the HIL simulator when a closed-loop PID position control and a LQR position and vibration control have been compared with the response of the real flexible-link mechanism using the very same real-time controllers. In this way, it has also been shown that a HIL system can be successfully used for the tuning of control system parameters without involving the mechanism prototype, thereby increasing the safety and reducing the time involved in experimental tests by eliminating the frequent mechanical failures of the flexible-link mechanism.

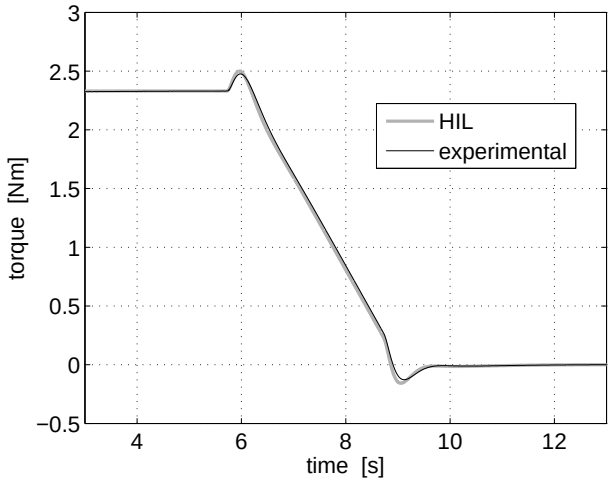

FIGURE 18. LQR CONTROL: HIL VS. EXPERIMENTAL RESULTS - APPLIED TORQUE

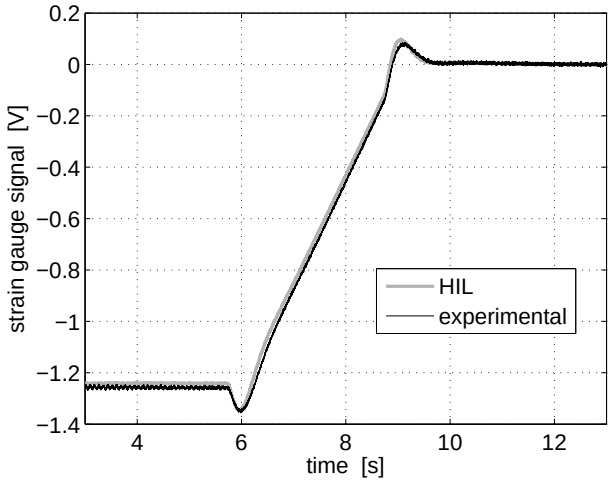

FIGURE 19. LQR CONTROL: HIL VS. EXPERIMENTAL RESULTS - STRAIN GAUGE SIGNAL

REFERENCES

[1] Dwivedy, A. K., Eberhard, P., 2006 "Dynamical analysis of flexible manipulators, a literature review", *Mechanism and Machine Theory* **41**

[2] Leitner, J., 1996, "Space Technology Transition Using Hardware in the Loop Simulation", *Proceedings of the 1996 Aerospace Applications Conference*, **2**, pp. 303-311,

[3] Hanselman, H., 1996, "Hardware-in-the-loop Simulation Testing and its Integration into a CACSD Toolset", *IEEE International Symposium on Computer-Aided Control System Design*, pp. 15-18, September

[4] Pritshow, G., Röck, S., 2004 "Hardware In the Loop Simu-

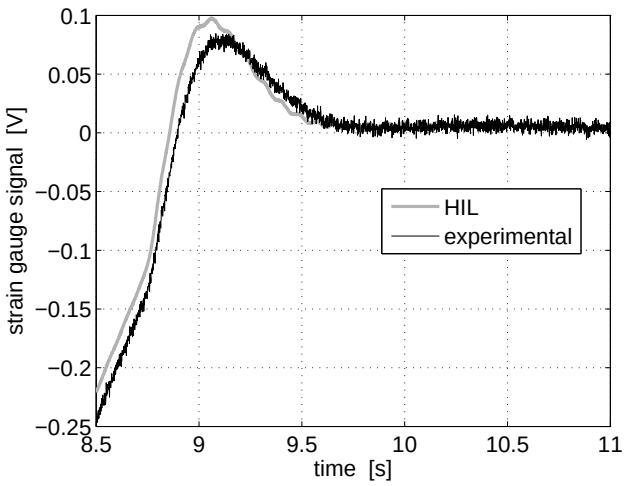

FIGURE 20. LQR CONTROL: HIL VS. EXPERIMENTAL RESULTS - STRAIN GAUGE SIGNAL, DETAILED VIEW OF SECOND TRANSIENT

lation of Machine Tools", *Ann CIRP* **53**(1), pp. 259-298

[5] Stoeppler, G., Menzel, T., Douglas, S., 2005 "Hardware-in-the-loop simulation of machine tools and manufacturing systems", *Computing & Control Engineering Journal* **16**(1), pp. 10-15

[6] Hu, X., 2005, "Applying Robot-in-the-loop Simulation to Mobile Robot Systems", *12th International Conference on Advanced Robotics ICAR 2005*

[7] Aghili, F., Piedboeuf, J.-C., 2002, "Contact dynamics emulation for hardware-in-loop simulation of robots interacting with environment", *Proceedings. ICRA '02. IEEE International Conference on Robotics and Automation*, **1**, pp. 523-529

[8] Chabra, R., Emami, M. R., 2008, "Concurrent Design of Robot Manipulators Using Hardware-in-the-loop Simulation", *2008 IEEE International Conference on Technologies for Practical Robot Applications (TePRA)*, Massachusetts, USA, November

[9] Martin A., Scot, E., Emami, M.R., 2006 "Design and development of robotic Hardware-In-the-Loop Simulation. Control, Automation, Robotics and Vision", *9th ICAR International Conference* **1**(6)

[10] Wasfy, T.M., Noor, A.K., 2003 "Computational strategies for flexible multibody systems" *Appl Mech Rev* **56**(6) February

[11] Boscariol, P., Gasparetto, A., Zanotto, V., 2010, "Active Position and Vibration Control of a Flexible Links Mechanism Using Model-Based Predictive Control", *Journal of Dynamic Systems, Measurement, and Control*, **132**(1) pp. 014506

[12] Boscariol, P., Gasparetto, A., Zanotto, V., 2009, "Vibrations Reduction in a Flexible Link Mechanism through the Synthesis of an MPC Controller" *IEEE International Conference on Mechatronics ICM 2009* Malaga, Spain, April

[13] Giovagnoni M., 1994 "A numerical and experimental analysis of a chain of flexible bodies" *ASME Journal of Dynamic Systems, Measurement and Control*, **113**, pp. 73-80

[14] Trevisani, A., Valcher, M.E., 2005 "An Energy-based Adaptive Control Design Technique for Multibody-Mechanisms wit Flexible-Links", *ASME/IEEE Transactions on Mechatronics* **10**, pp. 571-580

[15] Gasparetto A., Zanotto, V., 2006 "Vibration reduction in a flexible-link mechanism through synthesis of an optimal controller", *Meccanica* **41**(6), pp. 611-622

[16] Caracciolo, R., Richiedei, D., Trevisani, A., 2006 "Design and Experimental Validation of Piecewise-Linear State Observers for Flexible Link Mechanism", *Meccanica* **41**(6), pp. 623-637

[17] Gasparetto, A., 2004, "On the Modeling of Flexible-Link Planar Mechanism: Experimental Validation of an Accurate Dynamic Model" *ASME Journal of Dynamic Systems, Measurement and Control*, **126**(2)

[18] Franklin, F.G., Powell, F.G., Workman, M.L., 1990 *Digital Control of dynamic systems* 2nd*ed*. Addison Wesley